Modeling of Thin-Film $Cu(In,Ga)Se_2$ Solar Cells

F. Troni, F. Dodi, G. Sozzi, R. Menozzi
Department of Information Engineering, University of Parma
Parma, Italy
e-mail: fabrizio.troni@nemo.unipr.it

***Abstract*-We show results of numerical and compact modeling of poly-crystalline CIGS thin-film solar cells. We use numerical simulations as a benchmark to develop a simple, physics-based compact model of the behavior of the cell in the dark. We show that, while the single-crystal cell behavior can be accurately described by a two-diode model, when grain boundaries are present and active a four-diode model is required. Finally, we show results of the application of numerical simulations to the study of the cell degradation under damp heat stress conditions.**

I. INTRODUCTION

Thin-film solar cells based on $Cu(In,Ga)Se_2$ (CIGS) show record efficiencies among thin-film technologies, and are now experiencing the first phase of commercialization, with manufacturers introducing mass production processes yielding cells with efficiencies in the 10-16% range [1]-[3]. Lab specimens can provide power conversion efficiency as high as 20% [4], despite the poly-crystalline structure of the semiconductor thin film. The structure of the most popular cells features, from top to bottom, a ZnO transparent contact layer, an n-doped CdS buffer layer, a p-doped CIGS absorber layer, and a backside metal (Mo) contact sitting on a soda lime glass or flexible substrate.

Several papers were published on material growth, processing and characterization on one side, and on the performance of finished cells and modules on the other, but there is still a gap to fill in between: some of the specific features of CIGS cells, specifically those pertaining to the behavior of grain boundaries and heterojunctions, are still under debate, and a complete understanding of the relationship between material characteristics and cell behavior is not available yet. Since data about defects, band offsets, potential spikes, etc., at grain boundaries and interfaces are hard to obtain experimentally, and often indirect and speculative, some researchers have tried to bridge the gap using physical-level numerical simulations [5]-[8].

This work aims at using numerical simulations to investigate the specific features of these devices, with the ultimate goal of developing physics-based compact models for quick assessment of the performance of cells and modules under development at CNR-IMEM, Parma, Italy.

II. CIGS SOLAR CELL NUMERICAL MODELING

The behavior of defects at grain boundaries (GBs), in the grain interior (GI), and at hetero-interfaces is critical for the performance of CIGS solar cells. In particular it is known that: (i) the p-doped CIGS absorber has a columnar polycrystalline structure, with grains in the micrometer range; (ii) this polycrystalline structure does not have a disruptive effect on cell performance, probably due to charged defects and/or band offsets preventing the GBs from acting as effective recombination centers [9]; (iii) Cu-poor regions are likely to form at GBs and at the top CIGS interface, resulting in localized wider band-gap and valence band offset [10]. We focus on standard n-ZnO/n-CdS/p-$CuIn_{0.69}Ga_{0.31}Se_2$ cells (Fig. 1). Symmetry and periodicity allow to limit the simulated area to one grain boundary, provided that the grain size is reasonably uniform over the cell area. All the simulations are performed using Synopsys Sentaurus.

The cell behavior in the dark is described by the Poisson, electron and hole continuity and drift-diffusion equations. Recombination via deep defects follows the Shockley–Read–Hall (SRH) model. Deep traps are located in the GI (bulk acceptors), and at the GB (interface donors), the Cu-poor region at the GB may feature an increased band-gap totally localized on the valance band, ΔE_V (i.e., $\Delta E_C = 0$) [10]. Fig. 2 shows the energy band profile along a horizontal line in the vicinity of a GB (with $\Delta E_V = 0.2$ eV). The surface donors at the GB result in a downward bend of the energy bands that enhances the GB of electrons and depletes it of holes; in the presence of a valence band offset due to Cu depletion, the hole concentration is further reduced, which is beneficial to the cell in that it reduces non-radiative recombination at the GB. The full set of material parameters used in the simulations of the baseline cell is shown in Tab. I. The cell is illuminated by the standard AM1.5D solar spectrum.

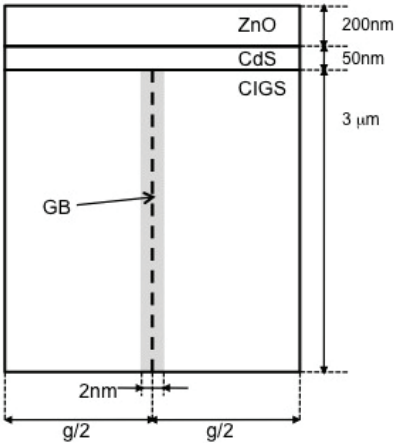

Fig.1 Structure of the simulated solar cell. g is the grain size. The gray region around the GB represents Cu-poor CIGS.

Work partly funded by CNR-IMEM, Parma, Italy, under the PED4PV project.

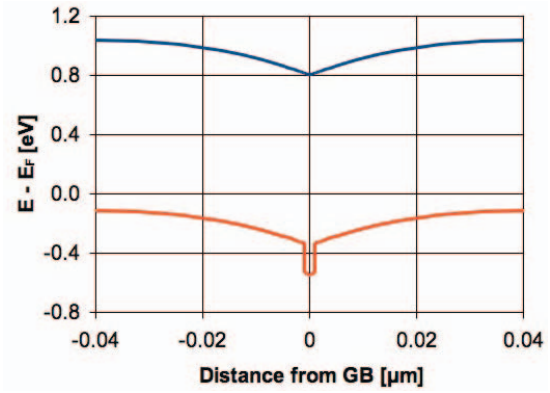

Fig. 2 Energy band profile along a horizontal line in the CIGS (see Fig. 1). The grain boundary hosts interface donors and is characterized by a valence band offset ΔE_V (0.2 eV in this example).

TABLE I
MATERIAL PARAMETERS

Layer	ZnO	CdS	CIGS
Eg [eV]	3.3	2.4	1.15
Doping [cm^{-3}]	$N_D = 10^{18}$	$N_D = 6 \cdot 10^{17}$	$N_A = 3 \cdot 10^{17}$
$\varepsilon/\varepsilon_0$	9	10	13.6
m_e/m_0	0.2	0.2	0.09
m_h/m_0	1.2	0.8	0.72
μ_e [$cm^2/(Vs)$]	100	100	100
μ_h [$cm^2/(Vs)$]	25	25	12.5
Bulk traps	**ZnO**	**CdS**	**CIGS**
Density [cm^{-3}]	10^{16}	10^{16}	10^{15}
Energy	midgap	midgap	midgap
σ_e [cm^2]	10^{-16}	10^{-15}	$2 \cdot 10^{-14}$
σ_h [cm^2]	10^{-13}	10^{-12}	$2 \cdot 10^{-14}$
GB traps	**Density**	**Energy [eV]**	$\sigma_e = \sigma_h$
Donor	$2 \cdot 10^{12}$ [cm^{-2}]	$E_V + 0.880$	10^{-15} [cm^2]

As an example, Fig. 3 shows the effect of the grain size g on the efficiency η (defined as the ratio between the output power at the maximum power point and the incident radiation power), for three different values of the valence band discontinuity at the GB, ΔE_V. As previously observed, the valence band offset at the GB hinders hole collection by the GB (see Fig. 2), thus reducing the recombination at GB defects; with $\Delta E_V = 0.4$ eV the GB is practically passivated. As expected, as the grain size increases, η tends to the single-crystal value > 17%. It is interesting to notice that a grain size variation in the 0.5-2 μm range, quite plausible for current manufacturing processes, results in a significant difference in η unless the GB is passivated by a large ΔE_V. Additional simulation results can be found in [11]. In the following the grain size is kept constant at 0.5 μm.

III. COMPACT MODELING OF THE DARK I-V CURVE

In the absence of defect-rich grain boundaries, the dark I-V curve of the cell can be satisfactorily described by a standard two-diode model, where a diode with ideality factor $n_I = 1$ describes the ideal diode current component, and a diode with $n_{SC} = 2$ accounts for the space-charge recombination current.

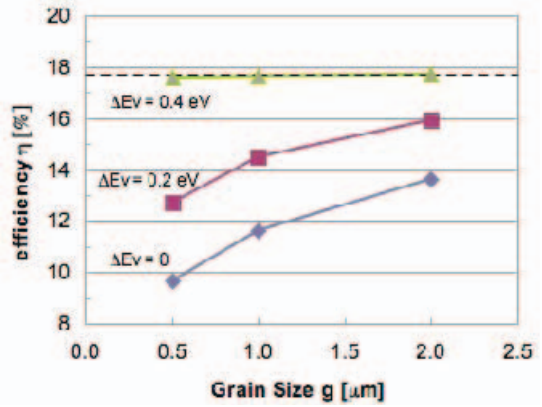

Fig. 3 Effect of CIGS grain size on efficiency, for different values of the GB valence-band discontinuity. The dashed line marks the efficiency of the single-crystal cell.

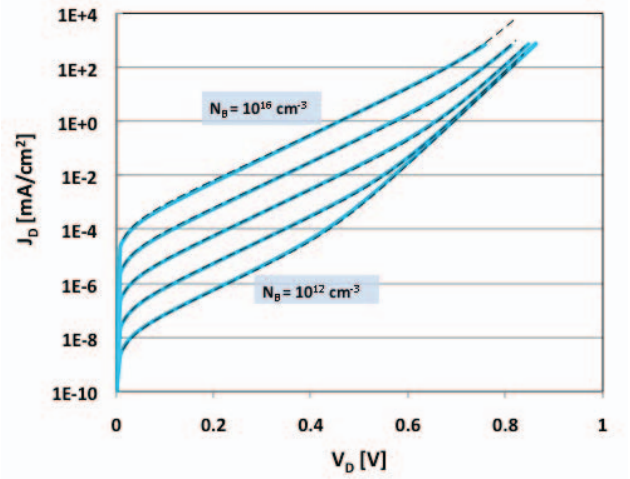

Fig. 4 Dark I-V curves for the single-crystal cell (no GBs), with different bulk defect densities N_B (10^{12}, 10^{13}, 10^{14}, 10^{15}, 10^{16} cm^{-3}) . The solid (blue) lines are numerical simulation results, the dashed (black) lines are obtained with the two-diode compact model.

Fig. 4 shows the perfect match between numerical simulations and the two-diode compact model for various bulk trap densities in the CIGS (N_B). The saturation currents of the two diodes are shown as a function of N_B in Fig. 5. The space-charge recombination saturation current J_{02} duly scales linearly with defect density; on the other hand, the ideal diode current J_{01} shows the transition between a short-base diode behavior at low N_B, where the current is nearly independent of the electron diffusion length (hence of N_B), to a long-base diode behavior at large N_B, where J_{01} grows with N_B due to shortening of the diffusion length.

The presence of defect-rich grain boundaries alters the picture with respect to the single-crystal case, the valence band discontinuity at the GB (ΔE_V) playing a key role. For $\Delta E_V = 0.4$ eV, the large valence band offset makes the semiconductor nearly intrinsic at the GB, and keeps holes away from the GB, thus locally inhibiting recombination via the interface defects. The conduction band dip caused by the charged interface donors (see Fig. 2) results in some channeling of the electron current along the GB at low bias; however, at high bias the current is almost uniformly distributed along the direction orthogonal to the GB. Consequently, the dark I-V curve is only marginally altered with respect to the single-crystal cell. This is shown in Fig. 6, where we compare the total dark current of the cell (solid line) with the electron current flowing outside the GB just below the CdS/CIGS interface, i.e., the p-n junction (dots):

the difference between the two is negligible, meaning that the situation is quite similar to the single-crystal case. Therefore, the two-diode compact model described above is still adequate.

The situation is dramatically different when $\Delta E_V = 0$. Here the band dip caused by the GB defects (Fig. 2) results in a much enhanced channeling of the current along the GB, as shown in the maps of Fig. 7. This remarkable difference is evident in the comparison between Fig. 6 and Fig. 8: the latter shows the dark current of the cell with $\Delta E_V = 0$ (solid line), together with the electron current flowing outside the GB just below the CdS/CIGS interface (dots), and the difference between the two (dashed line). Contrary to the situation of Fig. 6, here at moderate and high bias all of the electron current injected by the CdS cathode flows along the GB. Due to the large injected electron concentration, and since the GB is depleted of holes by the band dip caused by interface defects, high-injection conditions are reached quite early at the GB, with the dark I-V curve showing the typical $n_{HI} = 2$ ideality factor beyond $V_D = 0.5$ V.

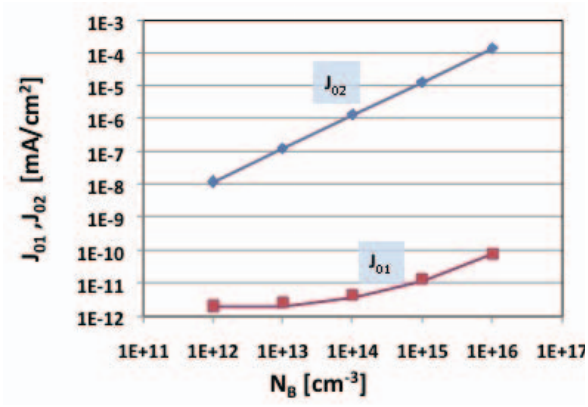

Fig. 5 Two-diode compact model parameters for the fit of Fig. 4, as a function of bulk trap density. J_{01} is the saturation current of the diode with ideality factor $n_I = 1$, J_{02} is the saturation current of the diode with ideality factor $n_{SC} = 2$.

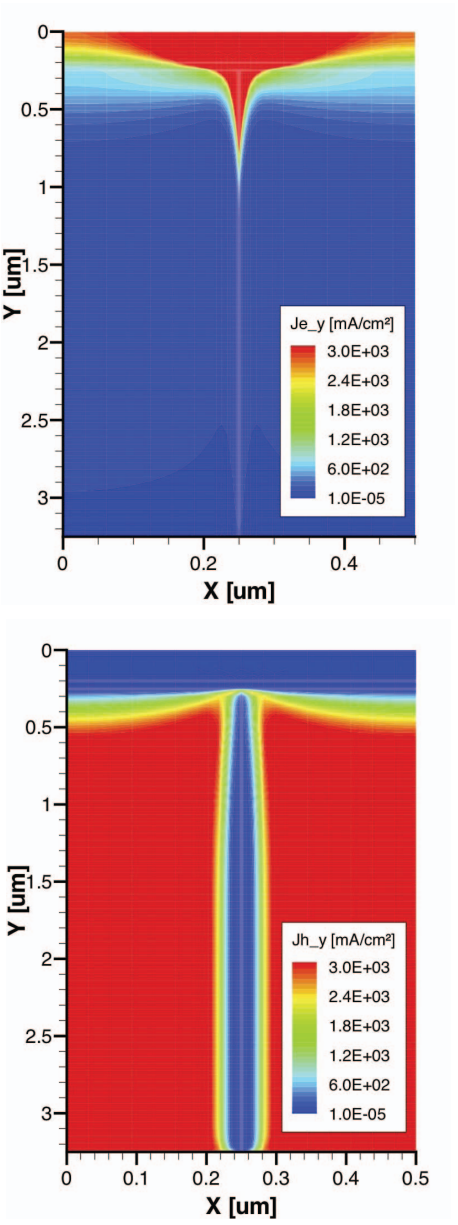

Fig. 7 Electron (top) and hole (bottom) current density map for a cell with $N_I = 2 \cdot 10^{12}$ cm^{-2} defects at the grain boundary and $N_B = 10^{14}$ cm^{-3} in the grain interior. $\Delta E_V = 0$. $V_D = 0.8$ V.

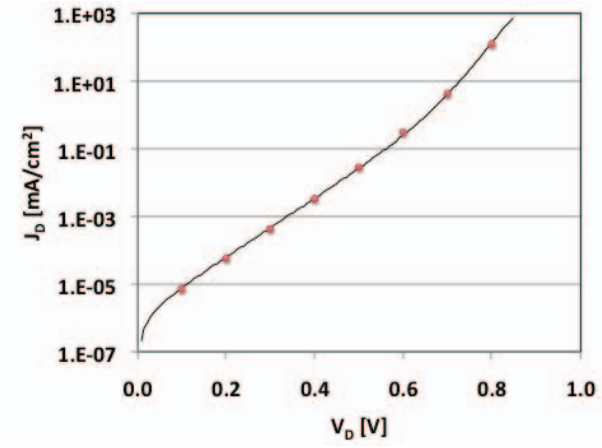

Fig. 6 Solid line: dark current characteristics for a cell with $N_I = 2 \cdot 10^{12}$cm^{-2} defects at the grain boundary, $\Delta E_V = 0.4$ eV, and $N_B = 10^{14}$ cm^{-3}. Dots: electron current flowing outside the GB just below the CdS/CIGS interface.

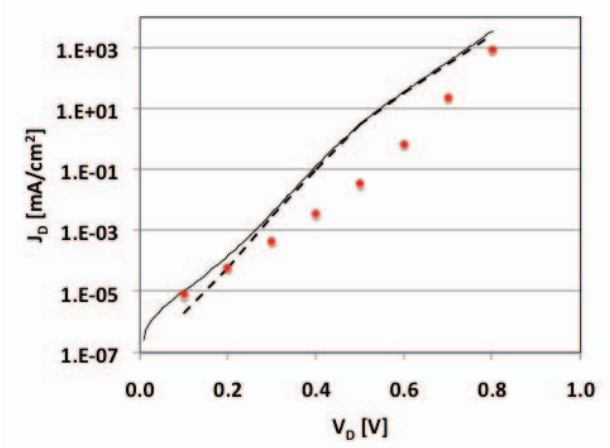

Fig. 8 Solid line: dark current characteristics for a cell with $N_I = 2 \cdot 10^{12}$cm^{-2} defects at the grain boundary, $\Delta E_V = 0$, and $N_B = 10^{14}$ cm^{-3}. Dots: electron current flowing outside the GB just below the CdS/CIGS interface. Dashed line: electron current flowing along the GB just below the CdS/CIGS interface.

A compact model physically representative of the cell with $\Delta E_V = 0$ at the GB must therefore include:

(1) a diode with ideality factor $n_I = 1$ describing the ideal current flowing outside the GB (dots in Fig. 8);
(2) a diode with $n_{SC} = 2$ describing the space-charge recombination current flowing outside the GB (dots in Fig. 8);
(3) a diode with ideality factor $n_{GB} = 1$ describing the ideal current component flowing along the GB (dashed line in Fig. 8); this diode must dominate the GB current at low-to-moderate bias (below about 0.5 V in Fig. 8);
(4) a diode with ideality factor $n_{HI} = 2$ describing the high-injection current flowing along the GB (dashed line in Fig. 8); this diode must dominate the GB current at moderate-to-high bias (above about 0.5 V in Fig. 8).

The simplest way of implementing this model is therefore a parallel connection of diodes (1) and (2) with a voltage-controlled current source $I_{3\text{-}4}(V_D)$ accounting for the current components (3) and (4); for example:

$$I_{3-4}(V_D) = \left(I_3(V_D)^{-1} + I_4(V_D)^{-1}\right)^{-1}.$$

This amounts to a 4-parameter model, the parameters being the saturation currents of diodes (1)-(4). An example of compact modeling of numerically-simulated dark I-V is given in Fig. 9.

IV. Numerical Simulation of Damp Heat Degradation

Long-term reliability is obviously a key factor for the success of any solar cell technology. In particular, damp heat (e.g., 85°C / 85% RH) is observed to be a critical condition for the long-term cell degradation. A numerical simulation model such as the one we developed can be usefully employed in this kind of investigation. As an example, we consider the change of defects distribution brought about by damp heat stress, as reported in [12] based on admittance spectroscopy measurements. Two defect are identified in [12]: N_1 is an interface defect undergoing activation energy increase during the stress, but not observed to influence the cell degradation, while N_2 is a bulk defect whose density and energy both increase upon stressing. We simulated these pre- and post-stress defect distributions (see Fig. 5 of [12] for details), and obtained the cell performance parameters shown in Tab. II, in qualitative agreement with published experimental observations.

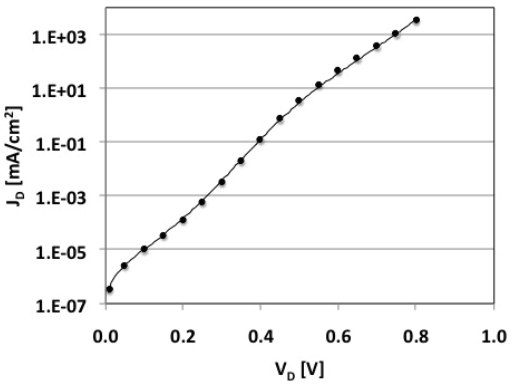

Fig. 9 Dark current characteristics for a cell with $N_I = 2 \cdot 10^{12} cm^{-2}$ defects at the grain boundary, $\Delta E_V = 0$, and $N_B = 10^{14} cm^{-3}$. Solid line: numerical simulation. Dots: 4-diode compact model; the 4 parameter values are: $J_{01} = 3 \cdot 10^{-11}$ mA/cm^2, $J_{02} = 1.5 \cdot 10^{-6}$ mA/cm^2, $J_{03} = 2.5 \cdot 10^{-8}$ mA/cm^2, $J_{04} = 4.5 \cdot 10^{-4}$ mA/cm^2.

TABLE II
Damp Heat Simulation

	Pre-Stress	Post-Stress
V_{OC} [V]	0.641	0.613
J_{SC} [mA/cm^2]	26.3	24.7
Fill Factor [%]	71.9	70.1
Efficiency [%]	12.1	10.6

V. Conclusions

We showed results of numerical as well as compact modeling of CIGS thin-film solar cells. The presence of defect-rich grain boundaries with possible band-gap modifications is a specific feature of these cells that must be accounted for in any physics-based model. We have used our numerical simulations as a benchmark to develop a simple, physics-based compact model of the behavior of the cell in the dark. While the single-crystal structure behavior can be accurately described by a standard two-diode model, when grain boundaries are present and active a four-diode model is required for a good match of the numerical simulation results. Further developments will include the compact modeling of the illuminated cell behavior. Finally, we have shown preliminary results of the application of numerical simulations to the study of the cell degradation under damp heat stress conditions.

References

[1] H. Komaki, Y. Kamikawa-Shimizu, T. Yoshiyama, K. Mizukoshi, K. Sakurai, S. Ishizuka, K. Matsubara, A. Yamada, H. Shibata, S. Niki, "Fabrication of integrated CIGS modules using the in-line three-stage process," *33rd IEEE Photovoltaic Specialists Conf.*, 2008.

[2] J. S. Britt, S. Wiedemann, U. Schoop, D. Verebelyi, "High-volume manufacturing of flexible and lightweight CIGS solar cells," *33rd IEEE Photovoltaic Specialists Conf.*, 2008.

[3] V. Kapur, A. Bansal, Z. Mantasser, J. Haber, A. Trivedi, D. Guevarra, D. Draganova, "'Ink-based' CIGS solar cells on lightweight Titanium foil," *34th IEEE Photovoltaic Specialists Conf.*, 2009.

[4] I. Repins, M. A. Contreras, B. Egaas, C. DeHart, J. Scharf, C. L. Perkins, B. To, R. Noufi, "19.9%-efficient ZnO/CdS/CuInGaSe$_2$ solar cell with 81.2% fill factor," *Prog. Photovolt.: Res. Appl.*, vol. 16, pp. 235-239, 2008.

[5] W. K. Metzger and M. Gloeckler, "The impact of charged grain boundaries on thin-film solar cells and characterization," *J. Appl. Phys.*, vol. 98, 063701, 2005.

[6] M. Gloeckler, J. R. Sites, W. K. Metzger, "Grain-boundary recombination in Cu(In,Ga)Se$_2$ solar cells," *J. Appl. Phys.*, vol. 98, 113704, 2005.

[7] K. Taretto and U. Rau, "Numerical simulation of carrier collection and recombination at grain boundaries in Cu(In,Ga)Se$_2$ solar cells," *J. Appl. Phys.*, vol. 103, 094523, 2008.

[8] U. Rau, K. Taretto, S. Siebentritt, "Grain boundaries in Cu(In,Ga)(Se,S)$_2$ thin-film solar cells," *Appl. Phys.* A, vol. 96, pp. 221-234, 2009.

[9] C. Persson and A. Zunger, "Anomalous grain boundary physics in polycrystalline CuInSe$_2$: the existence of a hole barrier," *Phys. Rev. Lett.*, vol. 91, 266401, 2003.

[10] M. J. Hetzer, Y. M. Strzhemechny, M. Gao, M. A. Contreras, A. Zunger, L. J. Brillson, "Direct observation of copper depletion and potential changes at copper indium gallium diselenide grain boundaries," *Appl. Phys. Lett.*, vol. 86, 162105, 2005.

[11] G. Sozzi, F. Troni, R. Menozzi, "Numerical analysis of the effect of grain size and defects on the performance of CIGS solar cells," Proc. CS-MANTECH Conf., pp. 353-356, Portland, OR, 17-20 May 2010.

[12] M. Schmidt, D. Braunger, R. Schaeffer, H. W. Schock, U. Rau, "Influence of damp heat on the electrical properties of Cu(In,Ga)Se$_2$ solar cells," *Thin Solid Films*, vol. 361-362, pp. 283-287, 2000.